Supplementary Text, Figures, and Tables

S1. Methods and data

Fine dust data

The IMPROVE definition of "Fine Soil" relies on the mass concentrations of common soil-derived elements (aluminium, silicon, calcium, iron, and titanium) and their normal oxides, along with a correction factor to account for other species such as water and carbonate [*Malm et al.*, 1994, 2004]. However, *Hyslop et al.* [2015] discovered that changes in analytical methods between 1995 and 2010 may have introduced spurious temporal trends in aluminium, silicon, and titanium. To assure the quality of the fine dust data over the 2000-2015 timeframe, we use the iron content of filter samples as a fine dust proxy, following the approach first proposed by *Hand et al.* [2016] and subsequently updated by *Achakulwisut et al.* [2017]. Here we calculate site-specific monthly mean fine dust concentrations as follows. (1) We neglect any sites at which $PM_{2.5}$-Iron is measured below the minimum detection limit on more than 20% of all days. (2) We screen out "high-combustion" days when the elemental carbon (EC) concentration exceeds a threshold value, defined here as the 2000-2015 EC monthly mean + 1 standard deviation for a given site. (3) If at least 50% of daily data are available for a given site and month, we calculate monthly mean $PM_{2.5}$-Iron concentrations from the daily values. (4) We approximate monthly mean fine dust concentrations as 6.5% $PM_{2.5}$-Iron, based on observed linear relationships between daily $PM_{2.5}$-Iron and IMPROVE "Fine Soil" from 2011 to 2015 (Figure S9). Since 2011, a new Panalytical XRF system has been used to determine elemental concentrations at all IMPROVE sites [*Hand et al.*, 2017]. *Lawrence and Neff* [2009] demonstrated that on average globally, the concentrations of most major elements in airborne dust tend to be similar to the composition of the upper continental crust. For iron, the observed global mean value is 3.6% (range of 1.3-7.8%). (5) Finally, we screen out sites with less than 50% monthly data for the 16-year time period. On average, the analytical uncertainties associated with our calculated monthly mean fine dust values are ~0.06% using error propagation. Further details behind our choice and method in using $PM_{2.5}$-Iron as a proxy for fine dust are provided in the Supplement of Achakulwisut et al. [2017].

Deriving observed relationships between fine dust and drought

We first examine the dominant spatial patterns of fine dust interannual variability across the Southwest using Empirical Orthogonal Function (EOF) analysis. We use a data matrix **S** (n x p) to represent the standardized anomalies of monthly mean fine dust concentrations over n monthly time steps and p sites. To fill in any missing values in the data matrix, we use the method of Data Interpolating Empirical Orthogonal Functions (DINEOF) [*Beckers and Rixen*, 2003; *Alvera-Azcárate et al.*, 2005]. This iterative EOF-based interpolation method has been shown to be a superior approach in terms of reconstruction accuracy [*Taylor et al.*, 2013]. Lastly, we perform EOF analysis via covariance matrix decomposition. The temporal covariance between different sites can be written mathematically as $\mathbf{A} = \mathbf{S}^{\mathrm{T}}\mathbf{S}/(n-1)$. The EOF spatial loadings are given by the eigenvectors of **A**, and the corresponding eigenvalues reflect the portion of total variance explained by each EOF. The principal components (PCs), which describe how the amplitude of each EOF varies with time, are derived by projecting **S** onto the eigenvectors of **A**.

We then examine the correlations of the most dominant mode (EOF1) with SPEI and other meteorological variables across the western United States and northern Mexico (15°-50°N, 125°-95°W). To focus on interannual variability, we detrend and deseasonalize monthly mean values for each site or grid point by first removing a linear trend obtained by simple regression, followed by subtracting the 2000-2015 monthly means. The residuals are hereafter referred to as fine dust anomalies. For the EOF analysis, we standardize the fine dust anomalies to assess regional patterns. The EOF-correlation analyses are performed by season - i.e., we use three continuous monthly mean fine dust or SPEI anomalies for 2000-2015 with a total number of 48 values in each time series.

Future projections of changes in fine dust concentrations

To calculate future changes in drought conditions, we use meteorological output from an ensemble of 22 CMIP5 climate models (Table S2) following the historical and two future scenarios, RCP2.6 and RCP8.5. We define 1996-2015 as our present-day period, and 2076-2095 as the future. Since the historical simulations end in the year 2005, we use 1996-2005 output from the historical simulation and 2006-2015 output from the RCP8.5 simulation for our present-day period. Actual global greenhouse gas emissions between 2006-2014 best matched the RCP8.5 scenario [*Fuss et al.*, 2014].

Health impacts assessment

The health endpoints assessed in this study are (1) premature mortality due to all-cause, cardiopulmonary disease, and lung cancer, and (2) hospitalizations due to cardiovascular and respiratory disorders. For mortality, we draw risk estimates from *Krewski et al.* [2009], the latest reanalysis of the American Cancer Society (ACS) study which considered the largest U.S. population cohort (aged ≥30 years) to date [*Pope III et al.*, 2002]. As in *Anenberg et al.* [2010], we derive the C-R coefficients using RRs for 1999-2000 from the random-effects Cox model analysis in *Krewski et al.* [2009], which adjusted for 44 individual-level and seven ecologic covariates from the nationwide analysis. Individual-level covariates include occupation, smoking habits, and alcohol consumption, while ecologic covariates include median household income and percentage of unemployment to control for confounding variables over time and space. A 10-μg m^{-3} increase in $PM_{2.5}$ was associated with 6% (95% CI, 4–8%), 13% (95% CI, 10–16%), and 14% (95% CI, 6–23%) increases in all-cause, cardiopulmonary, and lung cancer mortality. For morbidity, we use risk estimates from *Zanobetti et al.* [2009], who examined relationships between daily $PM_{2.5}$ levels and hospital admissions among 26 U.S. communities (aged ≥65 years). A 10-μg m^{-3} increase in $PM_{2.5}$ was associated with 2% (95% CI, 1–3%) increases in all-cardiovascular and all-respiratory admissions. Here we use annual mean $PM_{2.5}$ changes as a surrogate for daily changes, as *Fann et al.* [2012] suggested that this is unlikely to add appreciable bias given that the C-R functions are approximately linear across the air quality levels experienced by U.S. populations. Table S2 summarizes the health endpoints, epidemiological studies, and risk estimates used in this study.

For each premature mortality endpoint, we calculate present-day, age-standardized baseline incidence rates (for adults aged ≥30 years) using 1999-2015 averaged values for AZ, CO, NM, and UT from CDC Wonder (https://wonder.cdc.gov/ucd-icd10.html). For each morbidity endpoint, we calculate present-day age-standardized baseline incidence rates (for adults aged ≥65 years) using U.S. national values drawn from the EPA Environmental Benefits Mapping and Analysis Program (BenMAP) 2017 User's Guide (https://www.epa.gov/benmap/manual-and-appendices-benmap-ce). We approximate future values by applying the 2095:2015 ratio of the relevant age-standardized baseline incidence rate from the global integrated assessment model International Futures (IFs) (version 6.54;

www.ifs.du.edu). We use values from the "base case" scenario, in which inter-related policy issues regarding human development, economics, politics, and environmental sustainability evolve in a fashion aligned with historic trends and expert assessment of future changes (Hughes, 2004). We apply the weighted average of 2095:2015 cardiovascular and respiratory mortality ratios to project cardiopulmonary mortality rate, and the 2095:2015 malignant neoplasms ratio to project lung cancer mortality rate. Given that cause-specific hospitalization rates are not available, we approximate future values by applying the 2095:2015 ratio in cardiovascular and respiratory mortality rates to each relevant hospitalization endpoints.

We estimate the present-day U.S. Southwest population using 1996-2015 averaged population values for AZ, CO, NM, and UT from the U.S. Census Bureau (https://www.census.gov/topics/population/data.html). To calculate the number of adults aged ≥30 or ≥65 years to match risk estimates from epidemiological studies, we apply the relevant fractions drawn from the CDC Wonder database. To estimate future values, we use the projected growth rate in the total Southwest population (AZ, CA, CO, NM, NV, and UT) from the EPA's Integrated Climate and Land Use Scenarios (ICLUS v2; https://www.epa.gov/iclus/iclus-data-southwest-region). We use the 2095:2015 growth rate following the SSP2 scenario, which assumes medium levels of fertility, mortality, and international immigration, following the EPA's recommendation for the Climate Change Impacts and Risk Analysis (CIRA) project [*EPA*, 2017]. The 2095 age-group fractions are drawn from the IFs base case.

Final present-day and future baseline incidence rates are shown in Table S3. Final population estimates are shown in Table S4. In general, while age-specific rates of death and disease decrease in the future, increases in the percentages of the total population of adults aged ≥30 (from 63% to 68%) and ≥65 (from 12% to 28%) years result in overall increases in the age-standardized baseline incidence rates. The population increases from ~9.5 million to ~17 million for adults aged ≥30 years, and from ~1.8 million to ~6.8 million for adults aged ≥65 years.

S2. Sensitivity of SPEI to the choice of Potential Evapotranspiration (PET) equation

In choosing to rely on statistically downscaled CMIP5 data from the BCSD5 archive, we are limited to using the Thornthwaite (Thorthnwaite, 1948) or Modified Hargreaves (Droogers and Allen, 2002) equations in estimating the PET component of the SPEI. The widely used FAO Penman-Monteith equation requires additional variables not available from the BCSD5 archive.

The Thornthwaite equation, which is largely a linear rescaling of temperature to PET, has been shown to significantly overestimate PET with increasing temperatures beyond the mean of the baseline calibration period, and therefore inappropriate for use in global warming projections of drought (Hoerling et al., 2012; Cook et al., 2014). Droogers and Allen (2002) demonstrated that the Modified-Hargreaves, which relies on monthly mean daily maximum and minimum temperature and monthly total precipitation, is a robust alternative to the Penman-Monteith, especially when there are large uncertainties in additional variables required to calculate the Penman-Monteith (wind speed and relative humidity). We therefore present results calculated using the Modified-Hargreaves in our main analysis. The projected changes in SPEI02 for each model, season, and RCP scenario calculated using the Thornthwaite equation are shown in Figure S10. In general, the projected multi-model mean decreases in SPEI02 (and therefore increases in fine dust) are 25-51% smaller, and the health burdens are 35-39% smaller, when the Modified-Hargreaves is used instead of the Thorthwaite equation. The multi-model mean changes in SPEI02 and fine dust for each season and scenario are statistically significant from zero under both PET methods.

References

Achakulwisut, P., L. Shen, and L. J. Mickley (2017), What controls springtime fine dust variability in the western United States? Investigating the 2002-2015 increase in fine dust in the U.S. Southwest, *J. Geophys. Res. Atmos.*, *122*, doi:10.1002/2017JD027208.

Alvera-Azcárate, A., A. Barth, M. Rixen, and J. Beckers (2005), Reconstruction of incomplete oceanographic data sets using empirical orthogonal functions: application to the Adriatic Sea surface temperature, *Ocean Model.*, *9*(4), 325–346, doi:10.1016/j.ocemod.2004.08.001.

Anenberg, S. C., L. W. Horowitz, D. Q. Tong, and J. J. West (2010), An estimate of the global burden of anthropogenic ozone and fine particulate matter on premature human mortality using atmospheric modeling, *Environ. Health Perspect.*, *118*(9), 1189–1195, doi:10.1289/ehp.0901220.

Beckers, J. M., and M. Rixen (2003), EOF Calculations and Data Filling from Incomplete Oceanographic Datasets, *Am. Meteorol. Soc.*, *20*, 1839–1856.

Cook, B. I., Smerdon, J. E., Seager, R., and S. Coats (2014), Global warming and 21st century drying, *Clim. Dyn.*, *43*, 2607, https://doi.org/10.1007/s00382-014-2075-y.

Droogers, P., and R.G. Allen (2002), Estimating reference evapotranspiration under inaccurate data conditions, *Irrig. Drain. Syst.*, 16, 33–45. doi:10.1023/A:1015508322413.

EPA (2017), *Multi-Model Framework for Quantitative, Sectoral Impacts Analysis: A Technical Report for the Fourth National Climate Assessment*.

Fann, N., A. D. Lamson, S. C. Anenberg, K. Wesson, D. Risley, and B. J. Hubbell (2012), Estimating the National Public Health Burden Associated with Exposure to Ambient PM2.5 and Ozone, *Risk Anal.*, *32*(1), 81–95, doi:10.1111/j.1539-6924.2011.01630.x.

Fuss, S. et al. (2014), Betting on negative emissions, *Nat. Clim. Chang.*, *4*(10), 850–853, doi:10.1038/nclimate2392.

Hand, J. L., W. H. White, K. A. Gebhart, N. P. Hyslop, T. E. Gill, and B. A. Schichtel (2016), Earlier onset of the spring fine dust season in the southwestern United States, *Geophys. Res. Lett.*, *43*, 4001–4009, doi:10.1002/2016GL068519.

Hand, J. L., T. E. Gill, and B. A. Schichtel (2017), Spatial and seasonal variability in fine mineral dust and coarse aerosol mass at remote sites across the United States, *J. Geophys. Res. Atmos.*, *122*, 3080–3097, doi:10.1002/2016JD026290.Received.

Hoerling, M., Kumar, A., Dole, R., Nielsen-Gammon, J.W., Eischeid, J., Perlwitz, J., Quan, X. W., Zhang, T., Pegion, P., and M. Chen (2012), Anatomy of an extreme event,. *J. Clim.*, *26*(9), 2811–2832, doi:10. 1175/JCLI-D-12-00270.1.

Hyslop, N. P., K. Trzepla, and W. H. White (2015), Assessing the Suitability of Historical PM2.5 Element Measurements for Trend Analysis, *Environ. Sci. Technol.*, *49*(15), 9247–9255, doi:10.1021/acs.est.5b01572.

Krewski, D. et al. (2009), Extended follow-up and spatial analysis of the American Cancer Society study linking particulate air pollution and mortality., *Res. Rep. Health. Eff. Inst.*, (140), 5–114; discussion 115–36.

Lawrence, C. R., and J. C. Neff (2009), The contemporary physical and chemical flux of aeolian dust: A synthesis of direct measurements of dust deposition, *Chem. Geol.*, *267*(1-2), 46–63, doi:10.1016/j.chemgeo.2009.02.005.

Malm, W. C., J. F. Sisler, D. Huffman, R. A. Eldred, and T. A. Cahill (1994), Spatial and seasonal trends in particle concentration and optical extinction in the United States, *J. Geophys. Res.*, *99*(D1), 1347–1370, doi:10.1029/93JD02916.

Malm, W. C., B. A. Schichtel, M. L. Pitchford, L. L. Ashbaugh, and R. A. Eldred (2004), Spatial and monthly trends in speciated fine particle concentration in the United States, *J. Geophys. Res.*, *109*(D3), D03306, doi:10.1029/2003JD003739.

Pope III, C. A., R. T. Burnett, M. J. Thun, E. E. Calle, D. Krewski, K. Ito, and G. D. Thurston (2002), Lung cancer, cardiopulmonary mortality, and long-term exposure to fine particulate air pollution, *JAMA*, *287*(9), 1132–1141, doi:10.1001/jama.287.9.1132.

Taylor, M. H., M. Losch, M. Wenzel, and J. Schröter (2013), On the sensitivity of field reconstruction and prediction using empirical orthogonal functions derived from Gappy data, *J. Clim.*, *26*(22), 9194–9205, doi:10.1175/JCLI-D-13-00089.1.

Thornthwaite, C. (1948), An approach toward a rational classification of climate, *Geograph. Rev.*, 38(1):55–94.

Zanobetti, A., M. Franklin, P. Koutrakis, and J. Schwartz (2009), Fine particulate air pollution and its components in association with cause-specific emergency admissions, *Environ. Heal.*, *8*(1), 58, doi:10.1186/1476-069X-8-58.

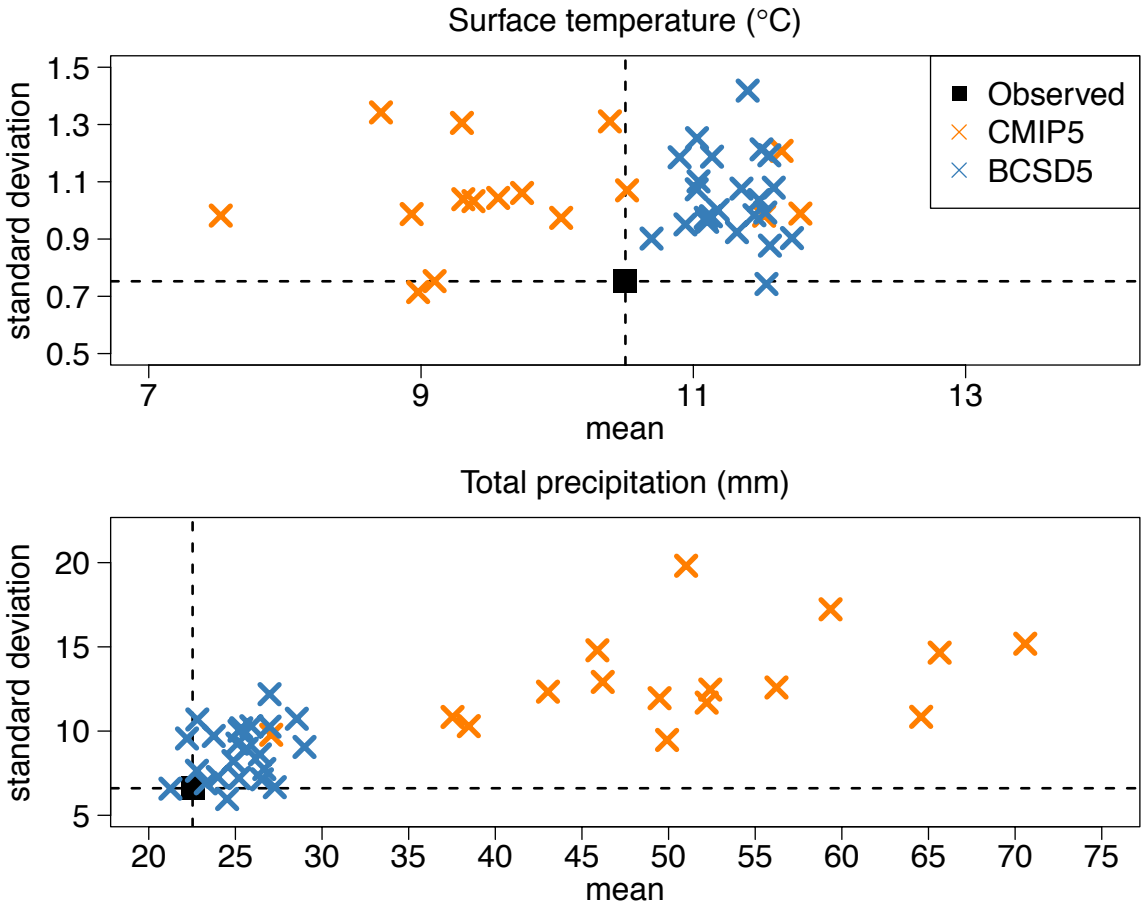

Figure S1. The 1996-2015 averaged mean and standard deviation of surface temperature and total precipitation averaged over the Southwest domain (31°-41°N, 115°-103°W). The black symbols and lines show observed values calculated using the Parameter-elevation Regression on Independent Slopes Model (PRISM) Climate Group database. Blue symbols show bias-corrected, statistically downscaled output from 23 CMIP5 models (BCSD5). Orange symbols denote the output from 16 CMIP5 models. See Table S1 for model details.

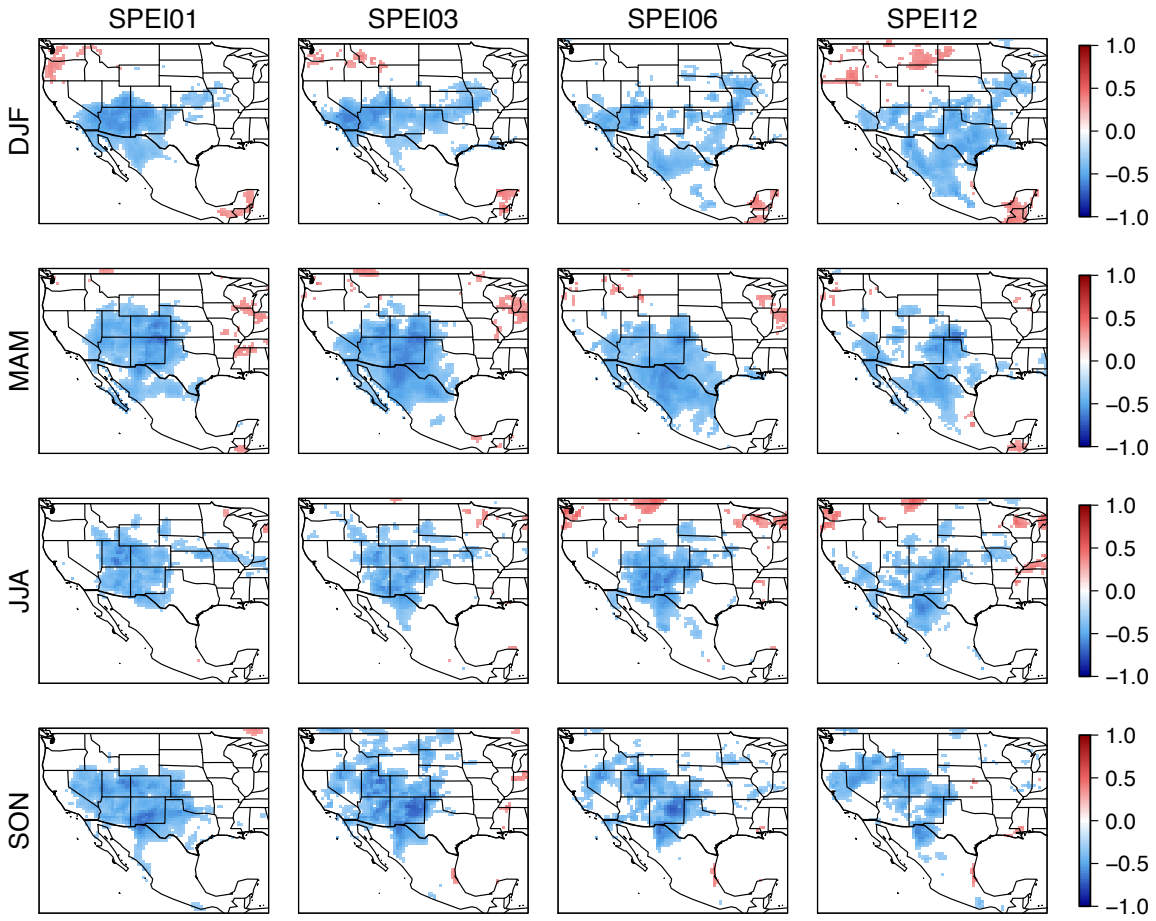

Figure S2. Correlations between the time series of the principal components of the 1st EOF mode of fine dust (PC1) and SPEI accumulated over 1, 3, 6, and 12 months for different seasons (DJF, MAM, JJA, and SON). Only those grid cells displaying statistically significant correlations ($p < 0.05$) are plotted.

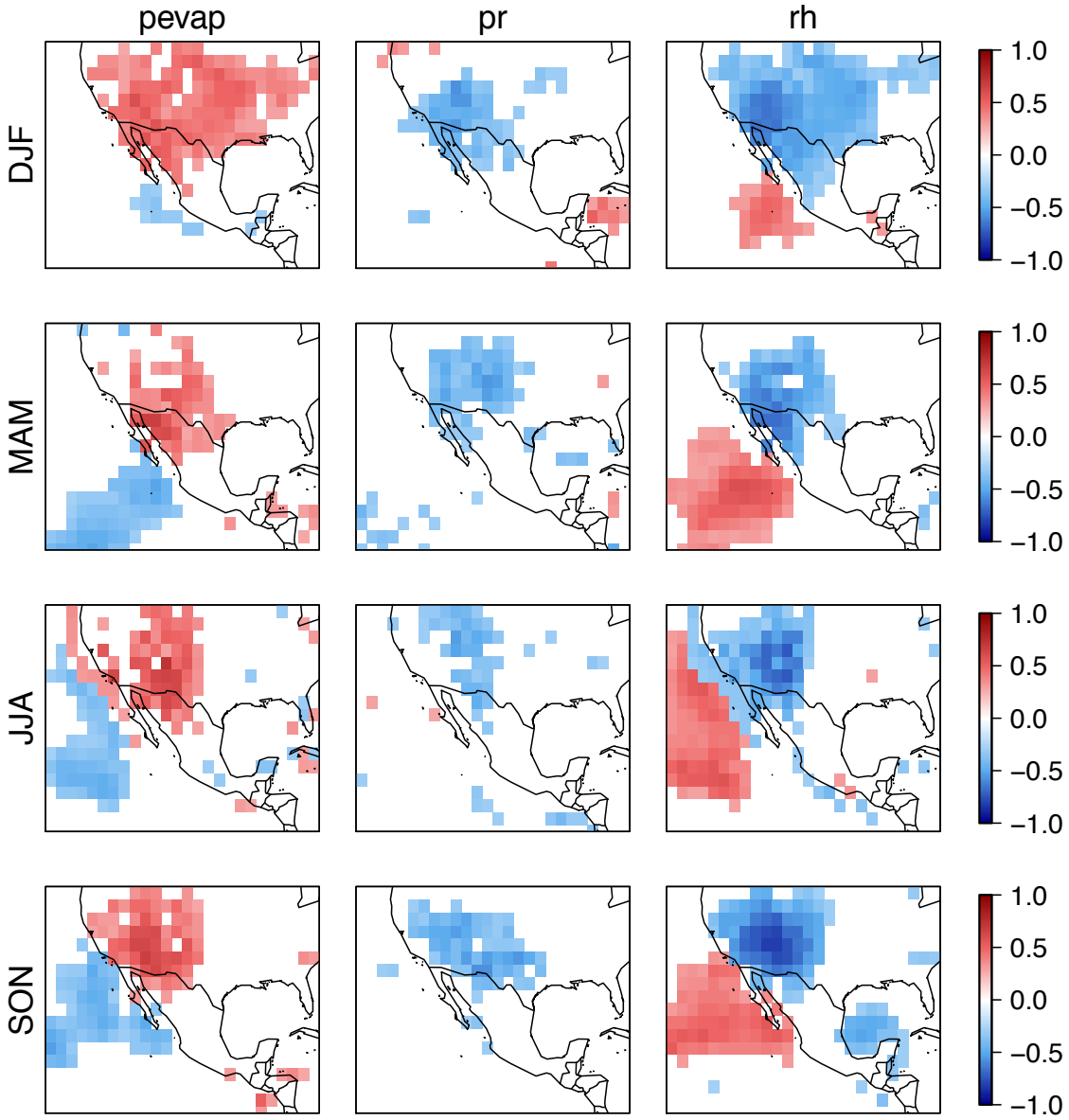

Figure S3. Correlations between the time series of the principal components of the 1st EOF mode of fine dust (PC1) and surface potential evaporation ("pevap"), precipitation ("pr"), and relative humidity ("rh") from the North American Regional Reanalysis for different seasons (DJF, MAM, JJA, and SON). Only those grid cells displaying statistically significant correlations ($p < 0.05$) are plotted.

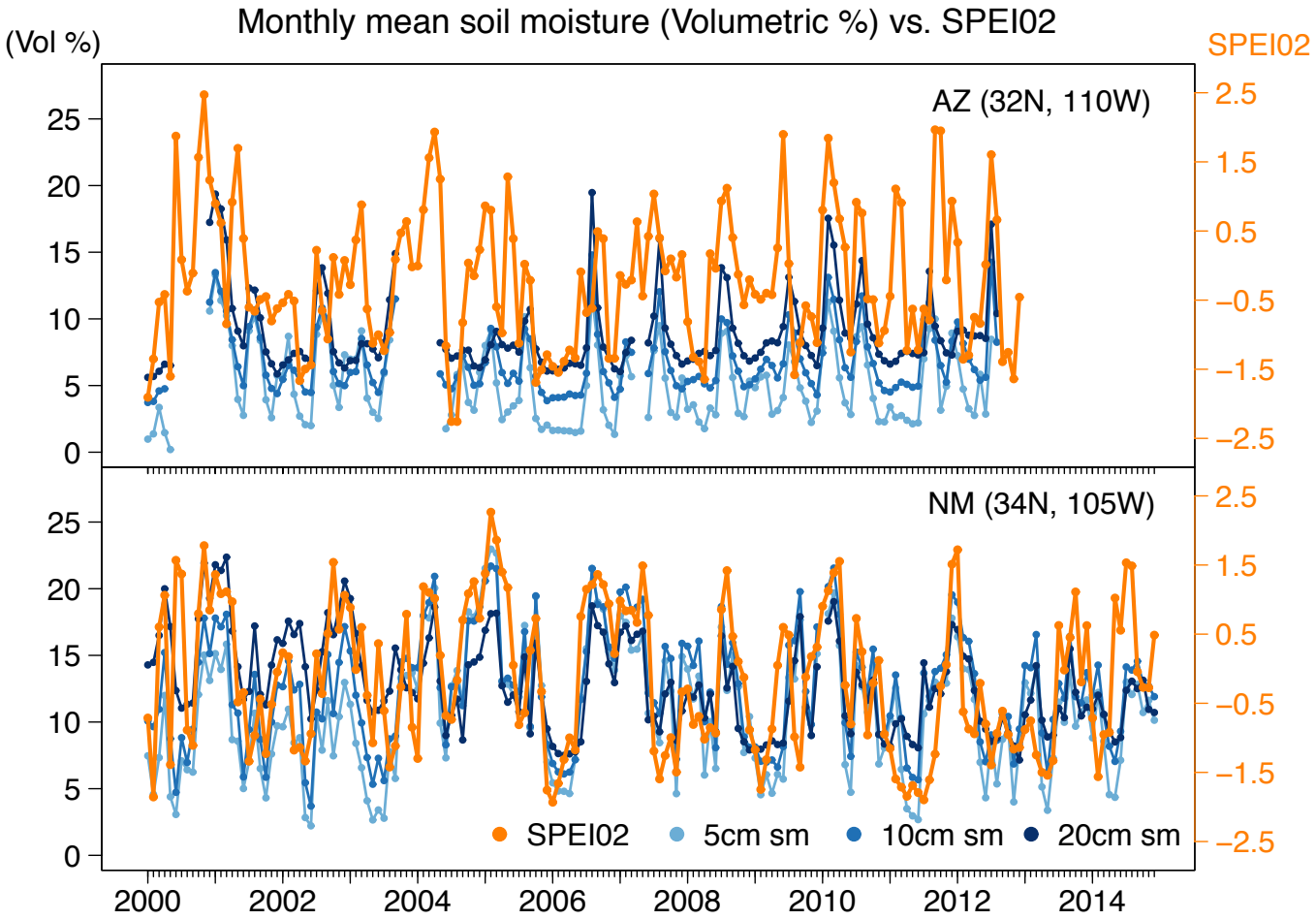

Figure S4. Timeseries of 2000-2014 monthly mean SPEI02 and soil moisture (volumetric %) at one site in Arizona (SCAN site #2026) and another in New Mexico (SCAN site #2015). The orange line shows SPEI02, and the blue lines show soil moisture measured at 5, 10, and 20 cm depths. The statistically significant correlations ($p < 0.05$) between SPEI02 and soil moisture range from 0.40-0.48 for the Arizona site, and 0.56-0.59 for the New Mexico site, depending on the soil depth.

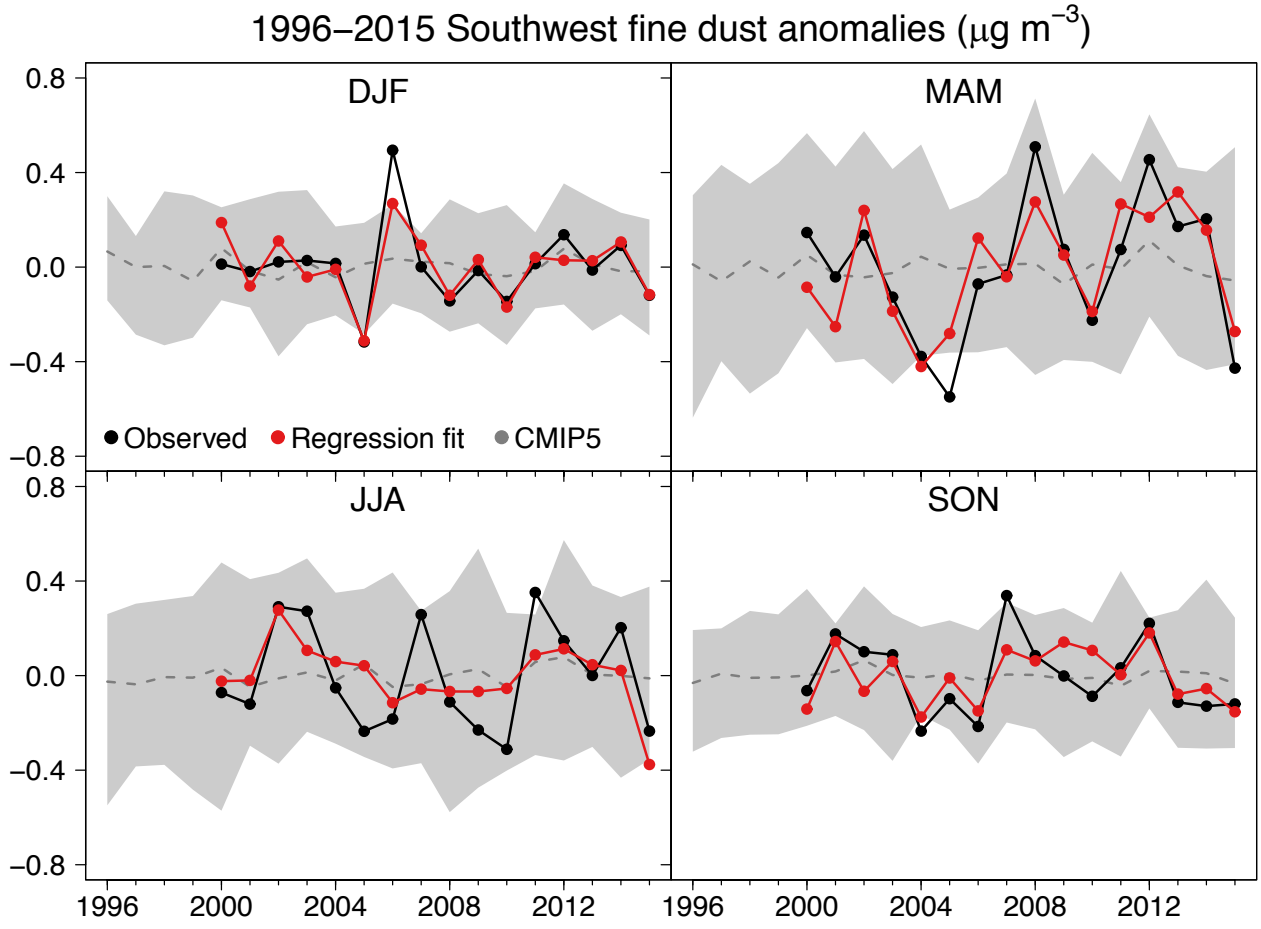

Figure S5. Timeseries of observed (2000-2015, black) and modeled (1996-2015, grey and red) seasonal mean fine dust anomalies averaged over the U.S. Southwest (here defined as Arizona, Colorado, New Mexico, and Utah). Observations represent the spatial average across 35 sites, calculated from detrended and deseasonalized monthly mean concentrations. Modeled values are calculated using a simple linear regression model with the 2-month Standardized Precipitation-Evapotranspiration Index (SPEI02) as the predictor (Table 1). Red lines denote fine dust anomalies calculated from a global SPEI database based on observed temperature and precipitation. The dotted gray lines show the multi-model means calculated using statistically downscaled meteorological output from an ensemble of 23 CMIP5 models, and gray shading shows the spread of the CMIP5 ensemble predictions. For all modeled cases, the SPEI02 values are averaged over different regional domains spanning the southwestern U.S. and northern Mexico for different seasons, as shown in Figure 1.

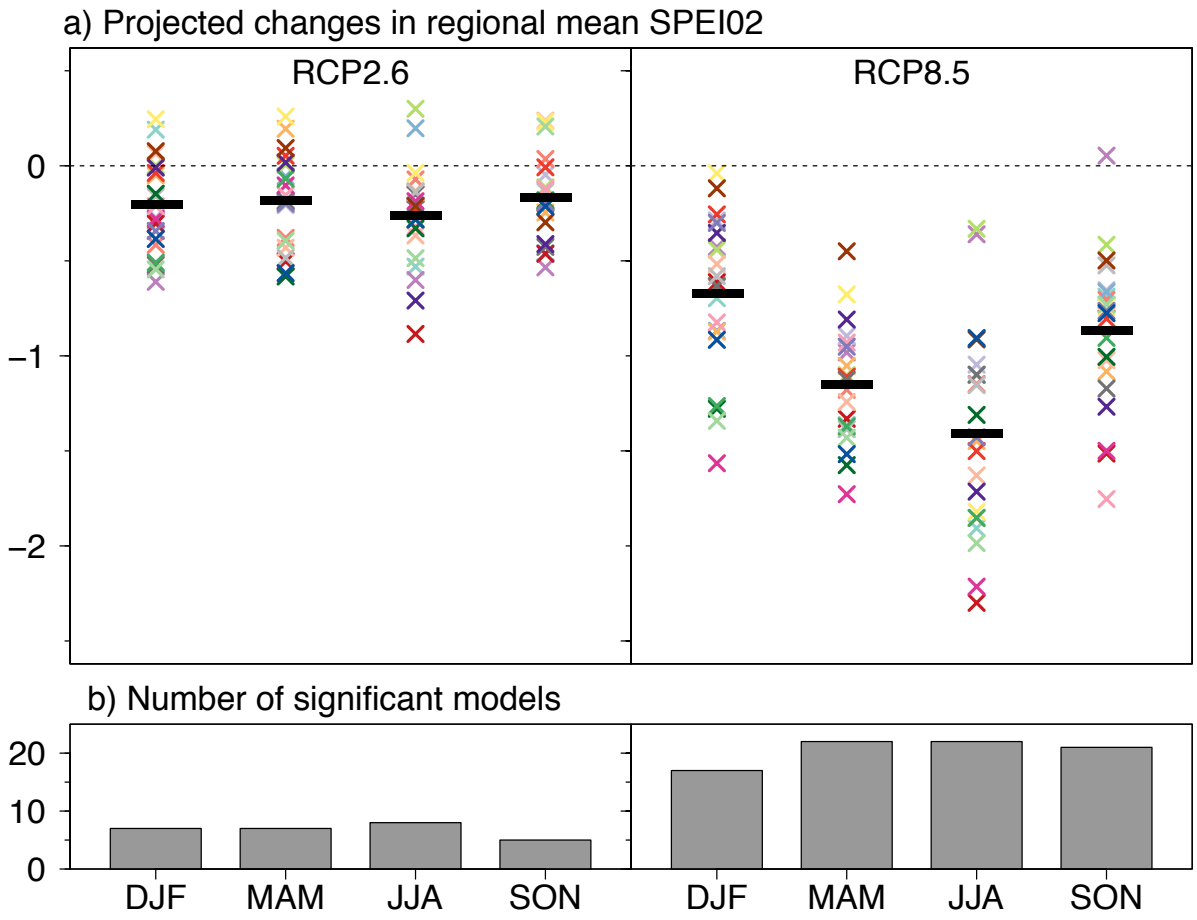

Figure S6. a) Projected changes in future (2076-2095) seasonal mean SPEI02 relative to the present day (1996-2015) under RCP2.6 and RCP8.5 scenarios. Different colored symbols denote results from different CMIP5 models, and the thick horizontal black lines show the multi-model means. b) The number of CMIP5 models that predict statistically significant decreases determined by a one-tailed Student's t-test ($p < 0.05$). For all seasons under both RCP scenarios, the multi-model mean decreases in SPEI02 are significantly different from zero, as determined by a Student's t-test ($p < 0.05$). We use statistically downscaled CMIP5 output.

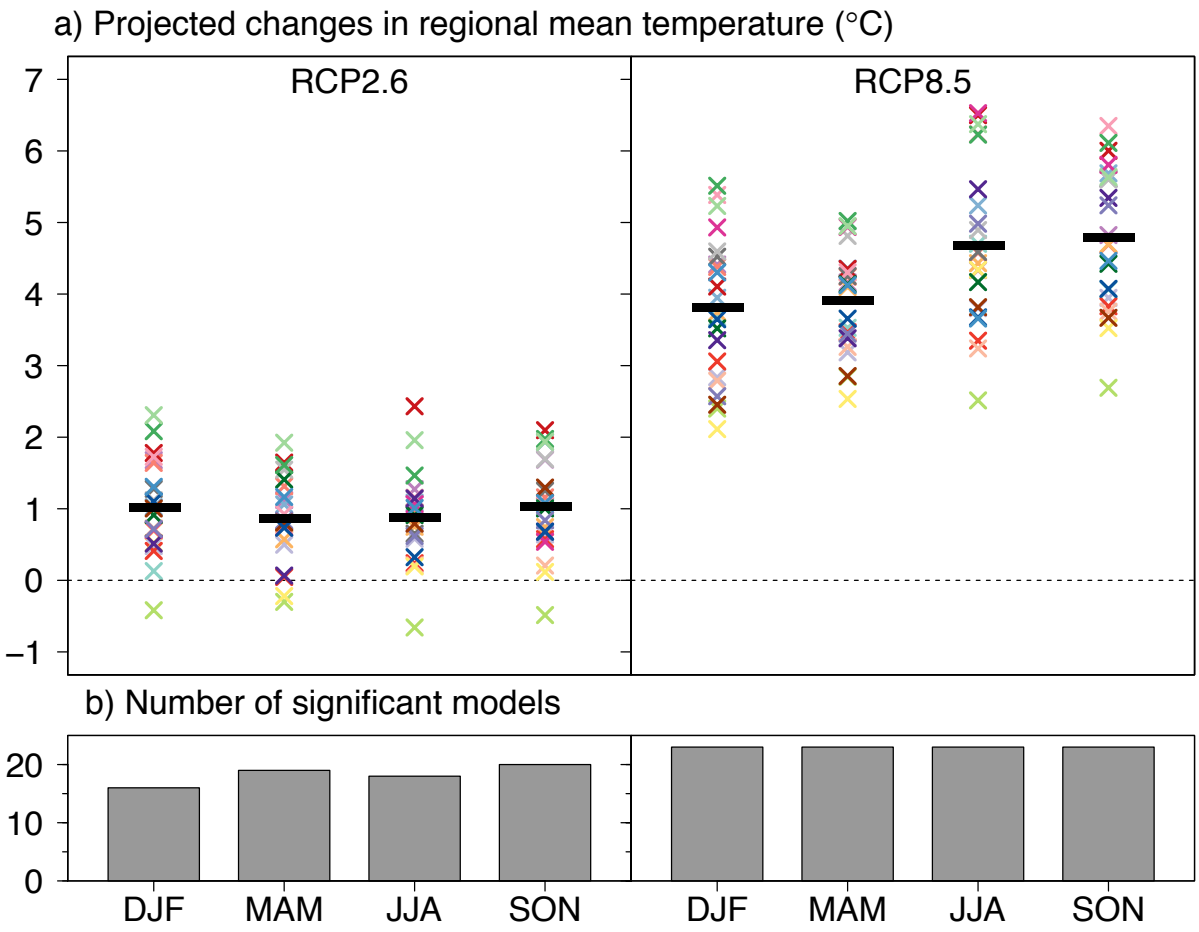

Figure S7. a) Projected changes in future (2076-2095) seasonal mean surface temperature relative to the present day (1996-2015) under RCP2.6 and RCP8.5 scenarios. The thick horizontal black lines show the multi-model means. b) The number of CMIP5 models that predict statistically significant increases determined by a one-tailed Student's t-test ($p < 0.05$). Different colored symbols denote results from different CMIP5 models. The multi-model mean increases for each season and scenario are all statistically significant, as determined by a Student's t-test ($p < 0.05$). We use statistically downscaled CMIP5 output.

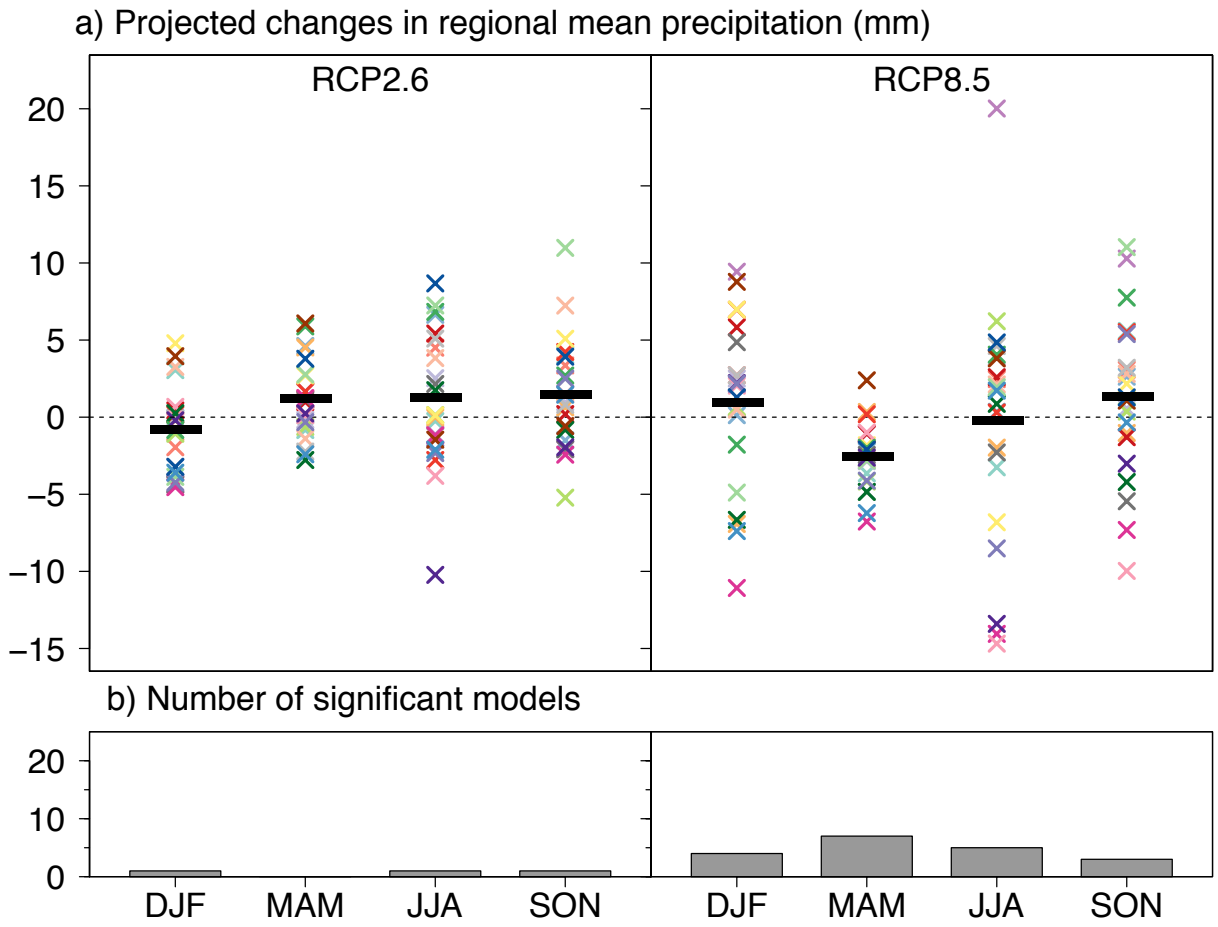

Figure S8. a) Projected changes in future (2076-2095) seasonal mean total precipitation relative to the present day (1996-2015) under RCP2.6 and RCP8.5 scenarios. The thick horizontal black lines show the multi-model means, which are significantly different from zero only for MAM under both RCP scenarios. b) The number of CMIP5 models that predict statistically significant decreases determined by a one-tailed Student's t-test ($p < 0.05$). Different colored symbols denote results from different CMIP5 models. We use statistically downscaled CMIP5 output.

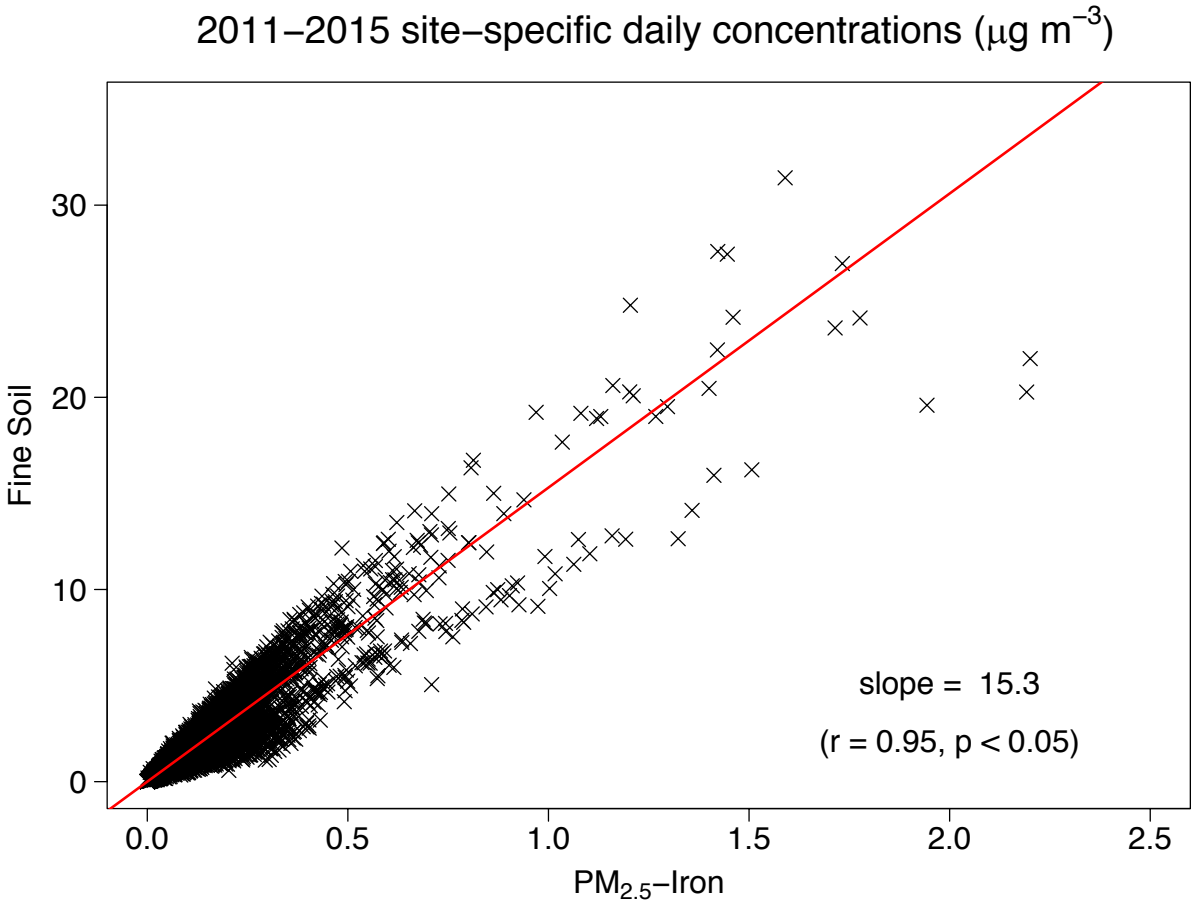

Figure S9. Daily fine soil vs. $PM_{2.5}$-Iron at 35 IMPROVE sites across the southwestern United States, with "high-combustion" days screened out, for 2011-2015. The IMPROVE definition of fine soil is 2.2×[Al] + 2.49×[Si] + 1.63×[Ca] + 2.42×[Fe] + 1.94×[Ti] (Malm et al., 1994, 2004). High-combustion days are those with daily element carbon (EC) concentrations above a threshold value, defined as the 2000-2015 EC monthly mean + 1 standard deviation for a given site.

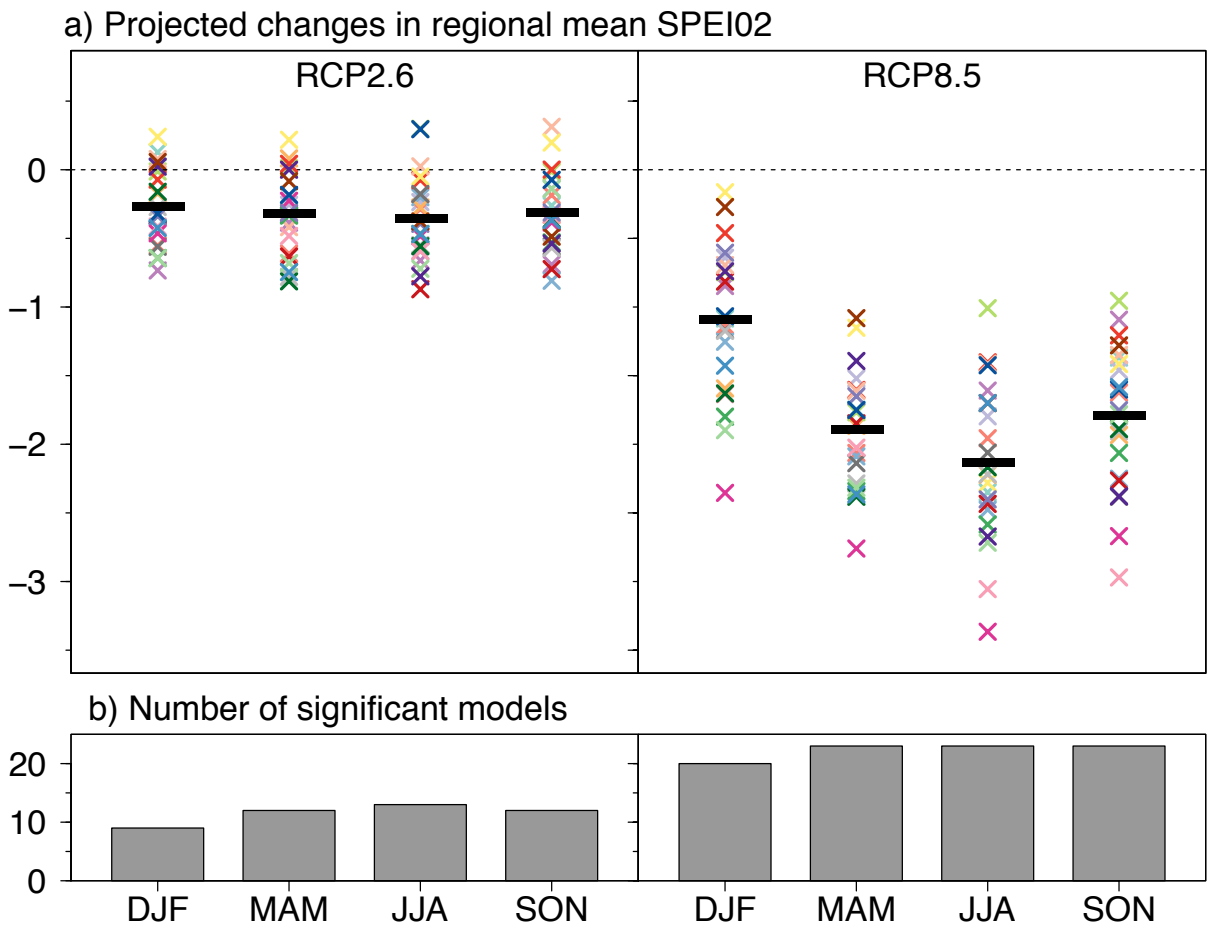

Figure S10. As in Figure S6 but using the Thornthwaite equation to estimate the Potential Evapotranspiration in calculating the SPEI.

Table S1. Drought classification based on the Standardized Precipitation Evapotranspiration Index (SPEI). Sources: Dai et al., 2011; Liu et al., 2014; Törnros and Menzel, 2014.

SPEI values	**Drought/Flood classification**
$SPEI \leq -2$	Extremely dry
$-2 < SPEI \leq -1.5$	Severely dry
$-1.5 < SPEI \leq -1$	Moderately dry
$-1 < SPEI \leq 0$	Mild drought
$0 < SPEI \leq 1$	Near normal wet
$1 < SPEI \leq 1.5$	Moderately wet
$1.5 < SPEI \leq 2$	Very wet
$SPEI > 2$	Extremely wet

Table S2. Models from the Coupled Model Intercomparison Project Phase 5 (CMIP5) used in this study. We use the bias-corrected and spatially-disaggregated projections of surface temperature and total precipitation from these models (Reclamation, 2014).

Model Name	Modeling Center/Group
BCC-CSM1-1	Beijing Climate Center, China Meteorological Administration
CanESM2[b]	Canadian Centre for Climate Modelling and Analysis
CCSM4	National Center for Atmospheric Research
CESM1-CAM5	Community Earth System Model Contributors
CSIRO-Mk3-6-0[a,b]	Commonwealth Scientific and Industrial Research Organization, Queensland Climate Change Centre of Excellence
FGOALS-g2	Laboratory of Numerical Modeling for Atmospheric Sciences and Geophysical Fluid Dynamics, Institute of Atmospheric Physics, Chinese Academy of Sciences, and Center for Earth System Science, Tsinghua University
FIO-ESM	The First Institute of Oceanography, State Oceanic Administration, China
GFDL-CM3[a]	NOAA Geophysical Fluid Dynamics Laboratory
GFDL-ESM2G[a]	
GFDL-ESM2M[a]	
GISS-E2-R[a,b]	NASA Goddard Institute for Space Studies
HadGEM2-AO[a,b]	Met Office Hadley Centre
HadGEM2-ES[a]	
IPSL-CM5A-LR[a,b]	Institut Pierre-Simon Laplace
IPSL-CM5A-MR[a,b]	
MIROC5[a,b]	Japan Agency for Marine-Earth Science and Technology, Atmosphere and Ocean Research Institute (The University of Tokyo), and National Institute for Environmental Studies
MIROC-ESM[a,b]	
MIROC-ESM-CHEM[a,b]	
MPI-ESM-LR[a,b]	Max-Planck-Institut für Meteorologie (Max Planck Institute for Meteorology)
MPI-ESM-MR[a,b]	
MRI-CGCM3[b]	Meteorological Research Institute
NorESM1-M[a,b]	Norwegian Climate Centre

[a] CMIP5 models from which we also analyze the original surface temperature and precipitation rates.

[b] CMIP5 models from which we also analyze the original 500 mb zonal wind fields.

Table S3. Log-linear concentration-response functions for $PM_{2.5}$-related health endpoints, as reported in epidemiological studies. For relative risk (RR) given in units of per 10 μg m^{-3}, the C-R coefficient, β, is derived as ln(RR)/10.

	Health Endpoint	**Study**	**Population Location**	**Population Age (years)**	**Relative Risk (RR) per 10 μg m^{-3} (95% CI)**
Premature mortality (due to change in annual average)	All-cause	Krewski et al. (2009)	Nationwide	≥30	1.06 (1.04-1.08)
	Cardiopulmonary				1.13 (1.10-1.16)
	Lung Cancer				1.14 (1.06-1.23)
Hospital admissions (due to change in 24-hour average)	All cardiovascular	Zanobetti et al. (2009)	26 U.S. communities	≥65	1.019 (1.013-1.025)
	All respiratory				1.021 (1.012-1.030)

Table S4. Summary of present-day and future baseline incidence rates for health endpoints considered in this study.

	Baseline mortality rates (deaths per 1000 y^{-1}) ≥ 25 y			**Baseline hospitalization rates (admissions y^{-1}) ≥ 65 y**	
	All-cause	**Cardiopulmonary**	**Lung Cancer**	**Cardiovascular**	**Respiratory**
Present-day	10.523	4.086	0.549	47.428	34.134
Future	22.085	9.311	0.937	109.426	74.350

Table S5. Present-day and future Southwest population estimates. Values in parenthesis show percentages of the total population. (See Section 2.2.4. for data sources.)

	Present	**Future**
≥30 years old	9.45 x 10^6 (63%)	16.6 x 10^6 (68%)
≥65 years old	1.80 x 10^6 (12%)	6.8 x 10^6 (28%)